A neuronal ensemble encoding adaptive choice during sensory conflict

Preeti Sareen[1], Li Yan McCurdy[1], Michael N. Nitabach[1, 2, 3, *]

[1]Department of Cellular & Molecular Physiology, Yale University, New Haven, CT, USA

[2]Department of Genetics, Yale University, New Haven, CT, USA

[3]Department of Neuroscience, Yale University, New Haven, CT, USA

*corresponding author: michael.nitabach@yale.edu

Abstract

Feeding decisions are fundamental to survival, and decision making is often disrupted in disease[1,2], yet the neuronal and molecular mechanisms of adaptive decision making are not well understood. Here we show that the neural activity in a small population of neurons projecting to the fan-shaped body in the central brain of *Drosophila* represents food choice during sensory conflict. We found that hungry flies made tradeoffs between appetitive and aversive values of food in a decision making task to choose unpalatable bittersweet food with high sucrose concentration over sucrose-only food with less sucrose. Using cell-specific optogenetics and receptor RNAi knockdown during the decision task, we identified an upstream neuropeptidergic and dopaminergic network that likely relays internal state and other decision relevant information, like valence and previous experience, to the fan-shaped body. Importantly, calcium imaging revealed that these fan-shaped body neurons were strongly inhibited by rejected food choice, suggesting that this neural activity is a representation of behavioral choice. FB response to food choice is modulated by taste, previous experience, and hunger state, which the fan-shaped body neurons likely integrate to encode choice before relaying decision information to downstream motor circuits for behavioral implementation. Our results uncover a neural substrate for choice encoding in a genetically tractable model to enable mechanistic dissection of decision making at neuronal, cellular, and molecular levels.

Keywords: decision making, conflicting sensory context, value integration, internal state, central complex, fan-shaped body

Main

Animals integrate food-related sensory information from their external environment with their internal state in order to make adaptive decisions. Often food-related sensory information is conflicting in valence. For example, *Drosophila* flies forage on decomposing fruits and, when hungry, must balance obtaining essential nutrition with avoiding toxins, pathogens, etc. As flies forage, sweet and bitter taste receptors on their legs and wings signal the presence of sweet nutritive food and bitter potential toxins[3]. Flies must adaptively weigh and integrate this conflicting information before consumption to enhance reproductive success. We investigated how value-based decisions are made in the brain of a hungry fly using an experimental paradigm in which freely walking flies sample and choose between different sweet-only and bittersweet foods (Fig. 1a). We quantified food choice and manipulated subsets of neurons while flies engaged in this decision task with conflicting taste information (Fig. 1a).

Hungry flies make tradeoffs when faced with conflicting sensory information

We tested wild-type flies deprived of food for different durations over a range of increasing concentration of sweet-only (sucrose) option against a constant bittersweet (sucrose + quinine) option. When choosing between a low sucrose concentration sweet-only option and a high sucrose concentration bittersweet option, flies prefer higher sucrose bittersweet (Fig. 1b). As sucrose concentration of the sweet-only choice increased, flies increasingly preferred it over bittersweet. This dose-dependent change in preference suggests that at higher sucrose concentrations of sweet-only option the caloric advantage in choosing a less palatable bittersweet food was lost (Fig. 1b). In the absence of bitter, flies always chose the sweeter option (Extended Data Fig. 1a). Flies equally preferred sweet-only and bittersweet option at 10-fold sucrose concentration difference (Fig. 1b, 50 mM vs. 500 mM sucrose+1 mM quinine). This equal-preference point was identical at all of the tested food deprivation durations (Fig. 1b). The equal-preference point depends on the sucrose concentration ratio between the two options and not absolute concentration (Extended Data Fig. 1b), indicating that there was no saturation of taste sensation at the concentrations used. These results indicate that hungry flies tradeoff the appetitive (sweet) and aversive (bitter) values of food in making feeding decisions.

To further understand decision making behavior, we also recorded location of flies at the end of decision task, and as expected, position preference mirrored ingested food preference (Fig. 1c). Social interaction between animals can have effects on decision making. To keep the task similar to fly's natural social environment, we used random proportions of males and females per trial. There was no effect of male-to-female ratio on ingested food preference (Fig. 1d). Previous studies have shown that group size can affect *Drosophila* behavior[4,5]. At equal-preference condition (21h deprivation, 50 mM sucrose), food preference and group size (Fig. 1e), food preference and percent of flies that ate (Fig. 1f), and percent of flies that ate and group size (Fig. 1g) were not correlated. There was also no significant prediction of preference index by group size or percent of flies that ate in a multiple regression model (Fig. 1h, Extended Table 1), indicating no interaction between these variables in the decision task.

A decision making neuronal ensemble converges on the fan-shaped body

During foraging, animals compute value estimates of internal hunger state and external sensory environment such valence of available foods, location of food, etc. Various neuromodulators regulate hunger dependent food intake[6-12], reward[13-16] or punishment[17], as well as memory[14,16,18]. The mushroom body is an insect central brain region involved in gustatory learning and memory[19,20] and valence encoding[21], and is thought to be a major center controlling higher-order behaviors[22-24]. The insect central complex is an evolutionarily conserved central brain region whose ellipsoid body and protocerebral bridge sub-regions have been implicated in navigation[25-32] and sleep[33-35]. The central complex fan-shaped body, a laminar neural sub-region, has been implicated in sleep[36-39] and ethanol preference[40,41]. The fan-shaped body was particularly interesting to us because several neuromodulators[42], their receptors[37,43,44], as well as dopaminergic inputs[45,46] co-localize in its layers. We hypothesized that value estimates of internal state and external environment from modulatory neurons will be required for integration by higher brain regions for decision making. To test this, we manipulated genetically targeted cell-specific neural expression using GAL4-UAS binary expression system[47]. We acutely optogenetically activated subsets of neurons using CsChrimson channelrhodopsin[48] while flies actively sampled and consumed food at the equal-preference condition (Fig. 1a, 1b, 21h food deprivation, 50 mM sucrose vs 500mM sucrose+1mM

quinine). It is not only activation of neurons but also inhibition that can modulate behavior. Therefore, for the next part of the screen, we optogenetically inhibited select genotypes from activation screen, using the anion-conducting channelrhodopsin GtACR1[49]. Genotypes were selected for inhibition screen based on the following pre-defined rules: a genotype with preference index lower than -0.3, or higher than 0.3, or a genotype with change in feeding during activation. This optogenetic interrogation of modulatory neurons and higher order brain regions revealed neuropeptidergic neurons (Leucokinin, Allatostatin A, NPF, DH44), subsets of dopaminergic neurons, and a narrow subset of fan-shaped body layer 6 neurons (FBl6) whose activation or inhibition significantly shifted food choice in the equal-preference condition (Fig. 2a).

Activation of Leucokinin (Lk) neurons suppressed feeding in food deprived flies (Fig. 2a, 2b left panel, Extended Fig. 2a-b), suggesting that Lk may relay metabolic state information. To confirm that Lk secreted by these neurons was the molecular basis of this feeding suppression, we simultaneously knocked down Lk expression with genetically encoded RNAi while optogenetically activating Lk neurons. The majority of flies consumed food during simultaneous Lk RNAi and activation, while almost no flies consumed when Lk neurons were activated without Lk RNAi. This indicates that Lk secretion mediates feeding suppression by Lk neurons (Fig. 2b left panel, Extended Fig. 2a-b). Optogenetic silencing of Lk neurons shifted preference towards bittersweet (Fig. 2a, 2b left panel, Extended Fig. 2a-b). Feeding suppression on Lk neuron activation implies a decrease in perceived hunger level of food deprived flies, which is consistent with implied increased perceived hunger level on Lk neuron inhibition leading to increased preference for high sucrose bittersweet food. Activation of Allatostatin A (AstA) neurons shifted the preference towards sweet, while inhibition shifted the preference towards bittersweet (Fig. 2a, 2c left panel). We confirmed that AstA was the molecular basis of this shift in preference by simultaneous AstA RNAi knockdown and activation of AstA neurons (Fig. 2c left panel). Flies preferred sweet on activation of NPF neurons, and this shift was abolished by simultaneous activation and NPF RNAi knockdown (Fig. 2a, 2d left panel). Activation of DH44 neurons had no significant effect, but inhibition shifted the preference towards bittersweet food (Fig. 2a, 2e left). Dopaminergic subsets

involved in aversive memory (Fig. 2a PPL1 γ2α'1)[50], taste conditioning (Fig. 2a PPL1 α3)[18], and long-term memory (Fig. 2a PAM α1)[14] also affected food choice. Activation of these dopaminergic subsets shifted the preference toward bittersweet (Fig. 2a). Activation of neurons from different mushroom body lobes, a brain region controlling higher-order behaviors, had no effect on preference. However, inhibition of a specific subset of fan-shaped body neurons, FBl6, shifted preference toward bittersweet (Fig. 2a, 3a left panel). Value estimates of internal state and external sensory environment, which are likely computed by modulatory neurons, are crucial for decision making. Fan-shaped body has co-localization of several neuromodulators and their receptors[37,42-46] and likely integrates the value estimates it receives from modulatory neurons.

To determine whether the neurons we identified in this optogenetic screen are connected in a behaviorally relevant ensemble, we employed a chemoconnectomics approach[51] exploring cell-specific genetically encoded RNAi knockdown of neuropeptide and dopamine receptors. Knockdown of neuropeptide or dopamine receptors in Lk neurons did not shift preference (Fig. 2b right panel), implying that Lk neurons receive food preference and hunger related information from other neurons. Dopaminergic Dop1R1 receptor RNAi in AstA neurons shifted preference towards sweet (Fig. 2c right panel), suggesting that AstA neurons receive food preference related dopaminergic inputs. Lkr and Dop1R1 receptor RNAi in NPF neurons shifted preference toward sweet (Fig. 2d right panel), suggesting that NPF neurons receive food preference relevant Lk and dopaminergic inputs. DopEcR receptor RNAi in DH44 neurons shifted preference toward bittersweet (Fig. 2e right panel), suggesting that DH44 neurons receive food preference relevant dopaminergic inputs.

Importantly, RNAi knockdown of Lkr, AstA-R1, or DH44-R1 receptors in FBl6 neurons shifted the preference toward bittersweet (Fig. 3a right panel), indicating that FBl6 neurons are modulated by these three neuropeptides to affect food choice. Furthermore, change in food preference on receptor RNAi in FBl6 mirrors change in food preference on respective neuropeptide neuron inhibition. For example, AstA-R1 receptor RNAi in FBl6 neurons should inhibit AstA input to FBl6, that is, have the effect that is equivalent of inhibiting AstA neurons. Consistently, both AstA-R1 receptor RNAi in FBl6 neurons (Fig.

3a right panel), and AstA neuron inhibition (Fig. 2c left panel) shifted food preference towards bittersweet. Similarly, both DH44-R1 receptor RNAi in FBl6 (Fig. 3a right panel) and DH44 neuron inhibition (Fig. 2d right panel) shifted preference towards bittersweet. Both Lkr receptor RNAi in FBl6 (Fig. 3a right panel), and Lk neuron inhibition (Fig. 2b right panel) also shifted preference towards bittersweet. RNAi of dopamine receptors in FBl6 had no effect (Fig. 3a right panel). This matrixed strategy mapped the neuromodulatory connections between nodes in the ensemble to control choice, and uncovered a previously unknown convergence node (FBl6) that is well positioned to integrate sensory, metabolic, and experiential information for decision making.

Fan-shaped body neurons encode choice

Value estimates of internal state like degree of hunger, and external environment like appetitive or aversive value of food (valence) and past experience, are integrated and transformed into choice. This raises the question of whether FBl6 neurons compute value estimates or integrate these estimates to encode choice. If FBl6 neurons estimated value of or encoded metabolic parameters such as hunger or satiety, manipulating their activity would be expected to influence feeding behavior. During FBl6 neural manipulation, majority of food deprived flies consumed food while majority of fed flies did not (Fig. 3b, Extended Table 1), demonstrating that hunger state is not affected by FBl6 neural activity. There was no significant difference in total amount of food consumed by flies during FBl6 neural manipulation compared to control flies (Fig. 3c, Extended Table 1). There was also no significant difference in the amount of sweet versus bittersweet food consumed per fly during FBl6 neural manipulation compared to controls (Fig. 3d, Extended Table 1). The shift in food preference during FBl6 inhibition (Fig. 3a left panel) was due to larger number of flies preferring to consume bittersweet over sweet food rather than each fly consuming larger quantity bittersweet food. Taken together, these results demonstrate that FBl6 does not encode or affect metabolic signals of hunger or satiety.

Next, we asked if activity of FBl6 neurons was inherently rewarding or aversive, that is, had inherent valence, which could shift food preference. To test this, we quantified place preference for illuminated versus dark parts of fly arena without food, during optogenetic manipulation of FBl6 neurons. FBl6

183 neural manipulation had no effect on preference for illuminated versus dark parts (Fig. 3e), demonstrating
184 that FBl6 activation or inhibition is neither inherently rewarding nor aversive.

185 Animals accumulate past experience to inform future decisions. We hypothesized that FBl6 integrates
186 hunger and food-related value estimates with experiential information for decision making. To understand
187 how past experience affects FBl6 activity, we recorded FBl6 neural activity in flies that had different
188 food-related experiences. Flies were presented taste stimuli from the equal-preference condition (Fig. 4a)
189 while ratiometric Ca^{2+} activity in FBl6 was measured using GCaMP6f[52] and tdTomato (Fig. 4a, b). First,
190 we tested the effect of hunger on FBl6 neural activity in naïve flies, i.e., flies that had not experienced the
191 decision task at all. FBl6 neurons of naïve food-deprived flies were strongly inhibited by the bittersweet
192 stimulus, but not sweet (Fig. 4d-e, naïve deprived). Flies often find bittersweet food aversive[20] and
193 inhibition of naïve fly FBl6 neural activity in response to bittersweet stimulus may be a representation of
194 rejected choice. Consistently, if FBl6 activity inhibition represents rejected food choice then neural
195 activity in naïve fed flies should be strongly inhibited by both sweet and bittersweet stimuli because fed
196 flies reject both foods in decision task (Fig. 3b). Indeed, FBl6 neurons of naïve fed flies showed strong
197 inhibitory response to both bittersweet and sweet stimuli (Fig. 4d-e, naïve fed).

198 Next, we asked, if similar to naïve flies, FBl6 neural activity also represents behavioral choice in flies
199 that experienced the decision task and made different food choices. FBl6 neurons of flies that chose sweet
200 food were strongly inhibited by rejected bittersweet stimulus but not by chosen sweet (Fig. 4d-e, chose
201 sweet). Correspondingly, FBl6 neurons of flies that chose bittersweet food were strongly inhibited by
202 rejected sweet stimulus but not by chosen bittersweet (Fig. 4d-e, chose bittersweet). FBl6 neurons of flies
203 that chose neither food, i.e. rejected both, were strongly inhibited by both bittersweet and sweet stimuli
204 (Fig. 4d-e, chose neither). Overall, FBl6 neural activity is always strongly inhibited by food that a fly
205 rejects, demonstrating that suppression of FBl6 activity is the neural representation of behavioral food
206 choice. This neural representation is modulated by taste (sweet vs. bittersweet), previous experience
207 (naïve vs. experience with two-choice conflict), as well as hunger state (naïve food deprived vs. fed) (Fig.
208 4d-e). FBl6 neurons likely receive these different types of information directly through AstA, DH44, and

Lk receptor signaling, and indirectly through NPF and dopamine pathways of the decision ensemble, for integrating them to form a representation of choice before sending information to downstream motor circuits for decision implementation (Fig. 4f).

Discussion

Animals make decisions about which foods to consume by integrating their internal physiological state with external sensory cues. Here we delineated a neuronal ensemble in *Drosophila* that underlies food-related decision making during sensory conflict between sweet and bittersweet food choices (Fig. 4f). Activating or silencing particular nodes in this ensemble shifts the decision balance between sweet and bittersweet food (Fig. 2b-e, 3a). This ensemble convergences on to FBl6 and FBl6 neurons likely integrate information from the upstream modulatory network to transform it into the neural representation of food choice (Fig. 4f).

Organisms must assess and assign value estimates to their external environment and internal state before integrating these estimates for adaptive decision making. Neuromodulatory subsets in the decision ensemble that we have identified have roles in hunger dependent food intake behavior, reward, valence, and memory. These modulatory neurons are well positioned to estimate value of the sensory environment and internal hunger state. For example, AstA neuron activation shifts food preference from carbohydrates to protein[6], while DH44 neurons sense sugars[53] and amino acids[11]. AstA and DH44 neurons may, therefore, convey food quality information to FBl6. NPF neuron activation is inherently rewarding[54] and may convey food valence information. Lk neurons have been implicated in nutrient sensing[9] and their activation suppresses feeding in food deprived flies (Fig. 2a-b), suggesting that internal metabolic state information may reach FBl6 through Lk/Lkr signaling. Dopaminergic subsets involved in aversive memory (PPL1 γ2α'1)[50], taste conditioning (PPL1 α3)[18], and memory (PAM α1)[14] also affected food choice (Fig. 2a) and may provide an error signal for predicting and updating value estimates similar to primate dopaminergic ventral tegmental area[55]. FBl6 neurons have axonal projections in the fan-shaped body[45,46], dense dendritic projections in the superior medial protocerebrum (SMP), and sparse dendritic projections in superior intermediate protocerebrum (SIP) and superior lateral protocerebrum (SLP)[45,46]

(Fig. 4g). In these higher brain regions, FBl6 receives synaptic inputs from dopaminergic neurons[38,39] that regulate sleep[38,39] and ethanol preference[41]. Interestingly, direct dopaminergic input to FBl6 through dopamine receptors did not influence food choice (Fig. 3a). Instead indirect dopaminergic inputs conveyed by neuromodulatory neurons regulated food choice (Fig. 2b-e). Mammalian studies provide converging evidence on multiple interconnected networks in frontal cortex and basal ganglia that compute and store value estimates of sensory environment and motor events in that environment required for decision making[55,56]. The neural ensemble described in this study has a similar framework of interconnected networks that potentially store, compute, and update value estimates for decision making.

A value integrator for food-related decision making requires estimates of taste identity, previous experience, and hunger state. FBl6 neuron activity is modulated by these parameters but it is not yet clear how the information brought to FBl6 from upstream network is integrated and transformed into the representation of behavioral choice before it is sent to downstream motor neurons for decision implementation (Fig. 4f). Decision making theories in mammals have traditionally focused on how values are represented in the brain[55,56], but how the brain integrates value information to make decisions when competing alternatives are present is still unclear[57]. Future investigations are required to identify and test proposed hypotheses of specific role of each node in the ensemble, how inputs from different nodes are integrated in FBl6, how this integration is transformed into the representation of choice, and which downstream motor circuits are involved in decision implementation.

References

1 Perugini, A., Ditterich, J. & Basso, M. A. Patients with Parkinson's Disease Show Impaired Use of Priors in Conditions of Sensory Uncertainty. *Curr Biol* **26**, 1902-1910, doi:10.1016/j.cub.2016.05.039 (2016).

2 Reiter, A. M., Heinze, H. J., Schlagenhauf, F. & Deserno, L. Impaired Flexible Reward-Based Decision-Making in Binge Eating Disorder: Evidence from Computational Modeling and Functional Neuroimaging. *Neuropsychopharmacology* **42**, 628-637, doi:10.1038/npp.2016.95 (2017).

3 Scott, K. Gustatory Processing in Drosophila melanogaster. *Annu Rev Entomol* **63**, 15-30, doi:10.1146/annurev-ento-020117-043331 (2018).

4 Ramdya, P., Schneider, J. & Levine, J. D. The neurogenetics of group behavior in Drosophila melanogaster. *J Exp Biol* **220**, 35-41, doi:10.1242/jeb.141457 (2017).

5 Rooke, R., Rasool, A., Schneider, J. & Levine, J. D. Drosophila melanogaster behaviour changes in different social environments based on group size and density. *Commun Biol* **3**, 304, doi:10.1038/s42003-020-1024-z (2020).

6 Hentze, J. L., Carlsson, M. A., Kondo, S., Nassel, D. R. & Rewitz, K. F. The Neuropeptide Allatostatin A Regulates Metabolism and Feeding Decisions in Drosophila. *Sci Rep* **5**, 11680, doi:10.1038/srep11680 (2015).

7 Lin, S., Senapati, B. & Tsao, C. H. Neural basis of hunger-driven behaviour in Drosophila. *Open Biol* **9**, 180259, doi:10.1098/rsob.180259 (2019).

8 Nassel, D. R. & Zandawala, M. Recent advances in neuropeptide signaling in Drosophila, from genes to physiology and behavior. *Prog Neurobiol* **179**, 101607, doi:10.1016/j.pneurobio.2019.02.003 (2019).

9 Zandawala, M. *et al.* Modulation of Drosophila post-feeding physiology and behavior by the neuropeptide leucokinin. *PLoS Genet* **14**, e1007767, doi:10.1371/journal.pgen.1007767 (2018).

10 Cannell, E. *et al.* The corticotropin-releasing factor-like diuretic hormone 44 (DH44) and kinin neuropeptides modulate desiccation and starvation tolerance in Drosophila melanogaster. *Peptides* **80**, 96-107, doi:10.1016/j.peptides.2016.02.004 (2016).

11 Yang, Z. *et al.* A post-ingestive amino acid sensor promotes food consumption in Drosophila. *Cell Res* **28**, 1013-1025, doi:10.1038/s41422-018-0084-9 (2018).

12 Wu, Q. *et al.* Developmental control of foraging and social behavior by the Drosophila neuropeptide Y-like system. *Neuron* **39**, 147-161, doi:10.1016/s0896-6273(03)00396-9 (2003).

13 Liu, C. *et al.* A subset of dopamine neurons signals reward for odour memory in Drosophila. *Nature* **488**, 512-516, doi:10.1038/nature11304 (2012).

14 Yamagata, N. *et al.* Distinct dopamine neurons mediate reward signals for short- and long-term memories. *Proc Natl Acad Sci U S A* **112**, 578-583, doi:10.1073/pnas.1421930112 (2015).

15 Lyutova, R. *et al.* Reward signaling in a recurrent circuit of dopaminergic neurons and peptidergic Kenyon cells. *Nat Commun* **10**, 3097, doi:10.1038/s41467-019-11092-1 (2019).

16 Huetteroth, W. *et al.* Sweet taste and nutrient value subdivide rewarding dopaminergic neurons in Drosophila. *Curr Biol* **25**, 751-758, doi:10.1016/j.cub.2015.01.036 (2015).

17 Riemensperger, T., Voller, T., Stock, P., Buchner, E. & Fiala, A. Punishment prediction by dopaminergic neurons in Drosophila. *Curr Biol* **15**, 1953-1960, doi:10.1016/j.cub.2005.09.042 (2005).

18 Masek, P., Worden, K., Aso, Y., Rubin, G. M. & Keene, A. C. A dopamine-modulated neural circuit regulating aversive taste memory in Drosophila. *Curr Biol* **25**, 1535-1541, doi:10.1016/j.cub.2015.04.027 (2015).

19 Kirkhart, C. & Scott, K. Gustatory learning and processing in the Drosophila mushroom bodies. *J Neurosci* **35**, 5950-5958, doi:10.1523/JNEUROSCI.3930-14.2015 (2015).

20 Masek, P. & Scott, K. Limited taste discrimination in Drosophila. *Proc Natl Acad Sci U S A* **107**, 14833-14838, doi:10.1073/pnas.1009318107 (2010).

21 Aso, Y. *et al.* Mushroom body output neurons encode valence and guide memory-based action selection in Drosophila. *Elife* **3**, e04580, doi:10.7554/eLife.04580 (2014).

22 Lewis, L. P. *et al.* A Higher Brain Circuit for Immediate Integration of Conflicting Sensory Information in Drosophila. *Curr Biol* **25**, 2203-2214, doi:10.1016/j.cub.2015.07.015 (2015).

23 Cohn, R., Morantte, I. & Ruta, V. Coordinated and Compartmentalized Neuromodulation Shapes Sensory Processing in Drosophila. *Cell* **163**, 1742-1755, doi:10.1016/j.cell.2015.11.019 (2015).

24 Tsao, C. H., Chen, C. C., Lin, C. H., Yang, H. Y. & Lin, S. Drosophila mushroom bodies integrate hunger and satiety signals to control innate food-seeking behavior. *Elife* **7**, doi:10.7554/eLife.35264 (2018).

25 Giraldo, Y. M. *et al.* Sun Navigation Requires Compass Neurons in Drosophila. *Curr Biol* **28**, 2845-2852 e2844, doi:10.1016/j.cub.2018.07.002 (2018).

26 Green, J., Vijayan, V., Mussells Pires, P., Adachi, A. & Maimon, G. A neural heading estimate is compared with an internal goal to guide oriented navigation. *Nat Neurosci* **22**, 1460-1468, doi:10.1038/s41593-019-0444-x (2019).

27 Honkanen, A., Adden, A., da Silva Freitas, J. & Heinze, S. The insect central complex and the neural basis of navigational strategies. *J Exp Biol* **222**, doi:10.1242/jeb.188854 (2019).

28 Kim, S. S., Rouault, H., Druckmann, S. & Jayaraman, V. Ring attractor dynamics in the Drosophila central brain. *Science* **356**, 849-853, doi:10.1126/science.aal4835 (2017).

29 Mathejczyk, T. F. & Wernet, M. F. Heading choices of flying Drosophila under changing angles of polarized light. *Sci Rep* **9**, 16773, doi:10.1038/s41598-019-53330-y (2019).

30 Seelig, J. D. & Jayaraman, V. Neural dynamics for landmark orientation and angular path integration. *Nature* **521**, 186-191, doi:10.1038/nature14446 (2015).

31 Sun, Y. *et al.* Neural signatures of dynamic stimulus selection in Drosophila. *Nat Neurosci* **20**, 1104-1113, doi:10.1038/nn.4581 (2017).

32 Turner-Evans, D. *et al.* Angular velocity integration in a fly heading circuit. *Elife* **6**, doi:10.7554/eLife.23496 (2017).

33 Liu, S., Liu, Q., Tabuchi, M. & Wu, M. N. Sleep Drive Is Encoded by Neural Plastic Changes in a Dedicated Circuit. *Cell* **165**, 1347-1360, doi:10.1016/j.cell.2016.04.013 (2016).

34 Liu, C. *et al.* A Serotonin-Modulated Circuit Controls Sleep Architecture to Regulate Cognitive Function Independent of Total Sleep in Drosophila. *Curr Biol* **29**, 3635-3646 e3635, doi:10.1016/j.cub.2019.08.079 (2019).

35 Guo, F., Holla, M., Diaz, M. M. & Rosbash, M. A Circadian Output Circuit Controls Sleep-Wake Arousal in Drosophila. *Neuron* **100**, 624-635 e624, doi:10.1016/j.neuron.2018.09.002 (2018).

36 Donlea, J. M., Pimentel, D. & Miesenbock, G. Neuronal machinery of sleep homeostasis in Drosophila. *Neuron* **81**, 860-872, doi:10.1016/j.neuron.2013.12.013 (2014).

37 Donlea, J. M. *et al.* Recurrent Circuitry for Balancing Sleep Need and Sleep. *Neuron* **97**, 378-389 e374, doi:10.1016/j.neuron.2017.12.016 (2018).

38 Liu, Q., Liu, S., Kodama, L., Driscoll, M. R. & Wu, M. N. Two dopaminergic neurons signal to the dorsal fan-shaped body to promote wakefulness in Drosophila. *Curr Biol* **22**, 2114-2123, doi:10.1016/j.cub.2012.09.008 (2012).

39 Pimentel, D. *et al.* Operation of a homeostatic sleep switch. *Nature* **536**, 333-337, doi:10.1038/nature19055 (2016).

40 Scaplen, K. M. *et al.* Circuits that encode and guide alcohol-associated preference. *Elife* **9**, doi:10.7554/eLife.48730 (2020).

41 Azanchi, R., Kaun, K. R. & Heberlein, U. Competing dopamine neurons drive oviposition choice for ethanol in Drosophila. *Proc Natl Acad Sci U S A* **110**, 21153-21158, doi:10.1073/pnas.1320208110 (2013).

42 Kahsai, L. & Winther, A. M. Chemical neuroanatomy of the Drosophila central complex: distribution of multiple neuropeptides in relation to neurotransmitters. *J Comp Neurol* **519**, 290-315, doi:10.1002/cne.22520 (2011).

43 Al-Anzi, B. *et al.* The leucokinin pathway and its neurons regulate meal size in Drosophila. *Curr Biol* **20**, 969-978, doi:10.1016/j.cub.2010.04.039 (2010).

44 Cavey, M., Collins, B., Bertet, C. & Blau, J. Circadian rhythms in neuronal activity propagate through output circuits. *Nat Neurosci* **19**, 587-595, doi:10.1038/nn.4263 (2016).

45 Kim, J. H. *et al.* The voltage-gated potassium channel Shaker promotes sleep via thermosensitive GABA transmission. *Commun Biol* **3**, 174, doi:10.1038/s42003-020-0902-8 (2020).

46 Qian, Y. *et al.* Sleep homeostasis regulated by 5HT2b receptor in a small subset of neurons in the dorsal fan-shaped body of drosophila. *Elife* **6**, doi:10.7554/eLife.26519 (2017).

47 Brand, A. H. & Perrimon, N. Targeted gene expression as a means of altering cell fates and generating dominant phenotypes. *Development* **118**, 401-415 (1993).

48 Klapoetke, N. C. *et al.* Independent optical excitation of distinct neural populations. *Nat Methods* **11**, 338-346, doi:10.1038/nmeth.2836 (2014).

49 Mohammad, F. *et al.* Optogenetic inhibition of behavior with anion channelrhodopsins. *Nat Methods* **14**, 271-274, doi:10.1038/nmeth.4148 (2017).
50 Berry, J. A., Cervantes-Sandoval, I., Nicholas, E. P. & Davis, R. L. Dopamine is required for learning and forgetting in Drosophila. *Neuron* **74**, 530-542, doi:10.1016/j.neuron.2012.04.007 (2012).
51 Deng, B. *et al.* Chemoconnectomics: Mapping Chemical Transmission in Drosophila. *Neuron* **101**, 876-893 e874, doi:10.1016/j.neuron.2019.01.045 (2019).
52 Chen, T. W. *et al.* Ultrasensitive fluorescent proteins for imaging neuronal activity. *Nature* **499**, 295-300, doi:10.1038/nature12354 (2013).
53 Dus, M. *et al.* Nutrient Sensor in the Brain Directs the Action of the Brain-Gut Axis in Drosophila. *Neuron* **87**, 139-151, doi:10.1016/j.neuron.2015.05.032 (2015).
54 Shao, L. *et al.* Dissection of the Drosophila neuropeptide F circuit using a high-throughput two-choice assay. *Proc Natl Acad Sci U S A* **114**, E8091-E8099, doi:10.1073/pnas.1710552114 (2017).
55 Sugrue, L. P., Corrado, G. S. & Newsome, W. T. Choosing the greater of two goods: neural currencies for valuation and decision making. *Nat Rev Neurosci* **6**, 363-375, doi:10.1038/nrn1666 (2005).
56 Lee, D., Seo, H. & Jung, M. W. Neural basis of reinforcement learning and decision making. *Annu Rev Neurosci* **35**, 287-308, doi:10.1146/annurev-neuro-062111-150512 (2012).
57 Tsetsos, K., Chater, N. & Usher, M. Salience driven value integration explains decision biases and preference reversal. *Proc Natl Acad Sci U S A* **109**, 9659-9664, doi:10.1073/pnas.1119569109 (2012).
58 Jenett, A. *et al.* A GAL4-driver line resource for Drosophila neurobiology. *Cell Rep* **2**, 991-1001, doi:10.1016/j.celrep.2012.09.011 (2012).
59 FlyLight, J.

Author contributions

P.S. conceptualized the study, designed and performed experiments, and analyzed data; L.Y.M. contributed to experimental design and fly dissection; P.S. and M.N.N. interpreted data; P.S. and M.N.N. prepared the manuscript with inputs from all authors.

Acknowledgements

We would like to thank Peter Niesman for help with calcium imaging data collection and Jason Braco for helpful discussions. Yichen Luo from John Carlson's lab provided useful information about taste delivery imaging rig. Tanya Wolff generously provided insights into fan-shaped body neuroanatomy. We would also like to thank Gerry Rubin and Tanya Wolff for sharing unpublished fly lines ss00208 and ss00225. These studies were supported in part by the National

Institute of Neurological Disorder and Stroke, National Institutes of Health (NIH) (RO1NS091070) and the National Institute of General Medical Sciences, NIH (RO1GM098932).

Methods

Fly husbandry

Flies were cultured on standard cornmeal medium on 12:12 light:dark cycle at 25ºC. w1118 lab stock was used as wild type. ss00208 and ss00225 unpublished split-GAL4 lines were a generous gift from Gerry Rubin. All genotypes and their sources are described in Extended Table 2. 2-5 day old flies were wet starved for 2-48 h (based on experiment design) on a wet Kimwipe with 1.5 ml distilled water. For optogenetic experiments, flies were food deprived for 21 h before testing on 0.4 mM all-*trans* Retinal (Cayman Chemicals) in 1% agar. Flies for RNAi knockdown and their controls were moved to 28ºC for 21 h the day before testing, i.e., during food deprivation, to induce strong RNAi. RNAi control was created for each GAL4 line by crossing the respective GAL4 to UAS-Valium (see Extended Table 2). All RNAi lines that we used were from Harvard TRiP project[1,2] and have been validated by independent groups (see Extended Table 2). Flies for simultaneous optogenetic and RNAi experiments were created using the genotypes mentioned in Extended Table 2. All experiments were conducted at Zeitgeber Time 3-6.

Two-choice assay and optogenetics

Sweet foods were made with different concentrations of sucrose and bittersweet foods with 500mM sucrose (Sigma) and 1mM quinine (Alfa Aesar or Beantown Chemicals, CAS#207671-44-1) dissolved in 1% agarose (AmericanBio) made in distilled water. 0.04% w/v red dye

(Sulforhodamine B, MP Biochemicals, CAS# 3520-42-1) and 0.02% w/v blue dye (Erioglaucine A, Alfa Aesar, CAS# 3844-45-9) were used for food coloring. Dye colors were alternated between sweet and bittersweet foods for each condition and there was no preference for one dye over the other at the concentrations used. Fly arenas were prepared by pouring agarose based foods in two-compartment petri-dishes (90-100 mm diameter) from Kord Valmark, EMS, or Fisher Scientific. Because of a thin physical barrier between the two compartments in the arena there was no diffusion between the two foods. Groups of 20-35 flies were aspirated and introduced into the arena 5-10 sec before the start of the experiment. All experiments were conducted in dark so that there was no effect of food color on preference. Arenas were placed on a platform with IR backlight for video recording using a Flea Pointgrey camera (FL3-U3-20E4C/M) at 15 fps. For optogenetics, we used high-power LEDs (Luxeon) placed adjacent to backlight IR LEDs (based on Janelia ID&F design) of 627 nm (for CsChrimson) and 520 nm (for GtACR1) that were controlled using Arduino Uno. For optogenetic screen, both red and green lights were pulsed at 100% max intensity, 50Hz, 25% duty cycle. For follow up experiments, CsChrimson experiments were conducted at 25% max intensity; GtACR1 follow up was done at screen condition. Light was pulsed for the entire duration of the experiment. At the end of the experiment, flies were anaesthetized using CO_2 and their belly color was recorded under a dissection microscope. Preference index (PI) was calculated as (no. of sweet food flies + 0.5 no. of both food flies) - (no. of bittersweet food flies + 0.5 no. of both food flies) / no. of total flies that ate, where negative PI would mean that more number of flies ate bittersweet food.

Food intake quantification

Food intake was quantified using spectrophotometry as previously described[3,4]. After recording belly color flies were frozen in 1.5 ml Eppendorf tubes at -20ºC until intake quantification (1-2 days). Flies from each trial were separately homogenized in distilled water (5 µl /fly) using a motorized pestle (BT Labsystems, BT703) for 1.5 min and centrifuged at 13000 rpm for 5 min. Absorbance of the debris-cleared 2 µl supernatant was measured on NanoDrop 2000 Spectrophotometer (Thermo Fisher Scientific) at 565 nm (for red dye) and 630nm (for blue dye). Flies that ate uncolored 1% agarose with 50mM sucrose were used as blank for baseline control. Red and blue dye concentrations were interpolated using their respective standard curves (GraphPad Prism) acquired from serial dilutions of single dyes in distilled water. Since we knew the number of flies that ate each color per trial, we could calculate per fly blue and red concentrations in the same solution.

Calcium imaging and data analysis

3-5 day old flies (naïve or after two-choice assay) were aspirated and positioned in a custom made fly holder in which they were glued using two-part transparent epoxy (Devcon). Only the top of fly head (for imaging) and the forelegs (for taste delivery) were outside the holder, while the rest of the fly, including proboscis were restrained in the fly holder. No anesthesia was used. A small piece of head cuticle was dissected and air sacs removed using a 30-gauge syringe needle and fine forceps, immediately followed by sealing the head capsule with a translucent surgical silicone adhesive (Kwil-Sil, WPI). Dissected fly was then placed in a humidified chamber for 15 min recovery before imaging.

Calcium imaging was performed on a Zeiss Axio Examiner upright microscope with 20x air objective and a Colibri module for LED control. tdTomato was excited at 555 nm (80%

intensity) and GCaMP6 at 470 nm (100% intensity). An image splitter (Photometrics DV-2) was used to split red and green channels and acquire simultaneous images for tdTomato and GCaMP6 using a Hamamatsu ORCA-R2 C10600 camera. Images were acquired at 5 fps with variable baseline (3 to 10 s required for stable tastant delivery) followed by tastant application to the forelegs, using a syringe, for 3 s and 4 s of no tastant. Excess tastant was wicked from the forelegs using absorbent tissue paper between each application. 10 s inter-trial interval was used during which all lights were off. Water was always applied first, followed by either sweet or bittersweet tastant. Sequence of sweet and bittersweet was alternated between flies. Sweet: 50 mM sucrose in distilled water; bittersweet: 500 mM sucrose + 1 mM quinine in distilled water. For flies that chose sweet in the two-choice behavior assay only trials with sweet as the first tastant were averaged and for flies that chose bittersweet, only trials with bittersweet as the first tastant were averaged.

Pixel intensities were extracted in Fiji followed by data analysis in MATLAB, both using custom written code. After background subtraction using Fiji's rolling-ball method (20 px), ROIs were manually drawn and saved on the tdTomato image, and superimposed on the GCaMP image (both reporters were expressed in the same neurons using the same driver) for mean ROI pixel intensity extraction. The saved intensity signals were then analyzed in MATLAB. tdTomato and GCaMP traces were individually corrected for photobleaching by fitting a single exponential function. Corrected GCaMP trace was then divided by the corrected tdTomato trace to obtain the ratiometric fluorescence trace (R). For relative fluorescence fold change ($\Delta R/R_0$) determination, baseline fluorescence (R_0) was calculated by averaging R over 2 s preceding tastant application. Peak $\Delta R/R_0$ was calculated during 4 s following tastant application.

493 *EM reconstruction*

494 Electron microscopy images were reconstructed from publically available Janelia FlyEM
495 hemibrain data using neuPRINT[5]. Neuron identities were confirmed in NeuronBridge[6] by cross-
496 referencing EM traced FBl6 neurons matched with light microscopy images of 84C10-GAL4
497 from FlyLight[7]. FBl6 mesh, whole FB mesh, and SMP, SIP and SLP brain region meshes were
498 used to depict brain regions with neural projection areas.

499

500 *Statistics*

501 All data were plotted in either Python or MATLAB using custom written code. Statistics were
502 carried out in GraphPad Prism. If all data passed Kolmogorov-Smirnov normality test, ANOVA
503 was conducted, otherwise Kruskal-Wallis test was conducted, both followed by appropriate post-
504 hoc tests. Details of statistics for each figure are provided in Extended Table 1. Sample sizes are
505 reported in parentheses next to dataset name in Extended Table 1.

506

507 **Figure legends**

508 **Fig. 1. Hungry flies make trade-offs between the appetitive and aversive value of food. a,**
509 Schematic of the two-choice decision making assay. Sweet and bittersweet foods are prepared in
510 agarose, mixed with food dyes (e.g. sweet blue and bittersweet red) and solidified in a circular
511 arena. Dye colors are counterbalanced within each condition. Flies are introduced into the food
512 arena in dark to walk, sample and consume freely for 5 min, while they are video recorded with
513 infrared (IR) backlight. At the end of the assay, flies are anaesthetized and their belly color is
514 recorded under a dissecting microscope indicating ingested food. Preference index is calculated
515 as (no. of sweet color flies+0.5 purple flies) - (no. of bittersweet color flies+0.5 purple flies)/total

no. of flies that ate. **b**, Preference index dose-response curves of wild-type (w1118) flies that underwent food deprivation for increasing durations show that flies make trade-offs between the sweet and bitter values of food and have equal-preference for both at a 10 fold sucrose concentration ratio (50 mM sucrose-only) between the sweet and bittersweet option. This equal-preference is dependent on concentration ratio between the two options (Extended Fig. 1b). For all further experiments, 21h food deprivation was used, which is highlighted in orange. **c**, Position preference index, i.e., sweet or bittersweet patch preference based on the location of the flies at the end of the assay matches ingested food preference, with equal-preference at 50 mM sucrose-only. **d,** Preferences of male and females within a group were indistinguishable at all the conditions tested. Preference index and group size per trial (**e**), preference index and % of flies that ate per trial **(f),** as well as % of flies that ate per trial and group size (**g)** were not correlated. **h,** Group size and % flies that ate did not significantly predict preference index in a multiple regression model, indicating no interaction between these variables. **b-d**, Plots show mean±95% CI, and violins depict full data distribution. Each violin has 10≤trials≤30 with mode=10. **e-h**, Heatmaps depict bivariate distribution visualized using a kernel density estimation procedure; darkest regions have higher data density. r^2 is the square of Pearson's coefficient. See Extended Table 1 for sample size and statistics.

Fig. 2. A decision making neuronal ensemble is revealed by combined optogenetics and RNAi knockdown. a, Cell-specific optogenetic activation and inhibition screen was performed at 21 h food deprivation and equal-preference condition (50 mM sucrose vs 500 mM sucrose+1 mM quinine). Neuronal subsets were genetically targeted using the GAL4-UAS binary expression system. CsChrimson (Chr) was used for activation and GtACR1 (Gt) for silencing.

Several neuropeptides, dopaminergic subsets, and a distinct subset of FB layer 6 neurons (FBl6) affected decision making based on significant difference in preference index compared to respective empty>Chr or empty>Gt controls. **b** (left), Leucokinin (Lk) neuron activation suppresses feeding in food deprived flies, while inhibition shifts the preference to bittersweet food. Simultaneous Lk RNAi and activation in Lk neurons abolishes activation effect. **b** (right), RNAi in Lk neurons of analogous receptors of other candidate neuromodulators has no effect. Lk manipulation effect is summarized in the adjacent schematic. **c** (left), Allatostatin A (AstA) neuron activation shifts preference to sweet while inhibition shifts it to bittersweet. Simultaneous AstA RNAi and activation abolishes activation effect. **c** (right), Dop1R1 RNAi in AstA neurons also shifts preference to sweet. **d** (left), NPF neuron activation shifts preference to sweet. This shift is abolished on simultaneous NPF RNAi and activation. **d** (right), Lkr and Dop1R1 RNAi in NPF neurons shifts preference to sweet. **e** (left), DH44 neuron activation has no effect while inhibition shisfts preference to bittersweet. **e** (right), DopEcR RNAi in DH44 neurons shifts preference to bittersweet. Neuropeptide manipulation effects for each panel are summarized in adjacent schematics. Plots show mean±95% CI, with violins depicting full data distribution; 5≤trials≤30 per violin, mode=10. Statistically different means are shown in different color. See Extended Table 1 for sample size and statistics. $p<0.00001$=****, $p<0.0001$=***, $p<0.01$=**, $p<0.05$=*.

Fig. 3. Fan-shaped Body layer 6 is the convergence node of a decision making ensemble. a (left), FBl6 neuron activation has no effect on preference however, inhibition shifts preference to bittersweet. **a** (right), Receptor RNAi knockdown of AstA-R1, DH44-R1, and Lkr in FBl6 also shifts preference to bittersweet. **b**, FBl6 activation or inhibition does not affect feeding initiation

in fed or food-deprived flies. **c-d**, Total consumption/fly is not different on FBl6 activation (**c**) or inhibition (**d**) compared to empty controls. Sweet and bittersweet consumption/fly is not different within the same group on FBl6 activation (**c**) or inhibition (**d**). **e**, There is no significant difference in place preference between FBl6 and empty control in an arena with illuminated and non-illuminated parts without food, indicating that neither activation nor inhibition of FBl6 is inherently rewarding or aversive. Plots show mean±95% CI, with violins depicting full data distribution. Statistically different means are shown in different color. See Extended Table 1 for sample size and statistics. $p<0.00001$=****, $p<0.0001$=***, $p<0.01$=**, $p<0.05$=*.

Fig. 4. Neural activity in FBl6 encodes food choice. a, Schematic of live animal calcium imaging during taste application of flies with different hunger state and experiences. Tastants from decision assay are applied to fly forelegs and changes in calcium responses are measured in the FBl6 using GCaMP6f. **b,** Neuronal expression of FBl6 reported by tdTomato for ratiometric imaging. Region of interest for fluorescence measurement is outlined in cyan. 84C10-GAL4 used to target FBl6 strongly and specifically targets FBl6 neurons[57,58], and shifts the preference to bittersweet on optogenetic inhibition (Extended Fig. 3b-d). **c,** EM reconstruction of example FBl6 neurons targeted by 84C10-GAL4 in the hemibrain with surface mesh for FBl6 shows projections restricted to FBl6. **d,** Ratiometric calcium responses, $\Delta R/R_0$, of flies with different hunger state and past experience. Sweet (50mM sucrose) and bittersweet (500 mM sucrose+1 mM quinine) tastants from equal-preference condition were applied for 3 s and neural response was quantified for 4 s post-stimulus application. Tastant application is indicated by gray background region. FBl6 neurons respond with strong inhibitory responses when behaviorally rejected tastant is presented (**d-e**). Calcium activity trace depicts mean $\Delta R/R_0$±95% CI. **e**, Peak

585 $\Delta R/R_0$ shows significant difference between response to rejected versus chosen tastant within
586 each fly condition. $p<0.05$=* (see Extended Table 1 for details on statistics). Points on graphs
587 represent mean±95% CI, with violins depicting full data distribution. **f**, EM reconstruction of
588 example FBl6 neurons targeted by 84C10-GAL4, with surface mesh for whole FB showing
589 surface meshes for higher brain regions to which FBl6 neurons project. **g,** Schematic of the
590 decision making ensemble converging on to FBl6. FBl6 activity is the neural representation of
591 behavioral food choice. This activity is modulated by taste, previous experience, and hunger
592 state. FBl6 neurons likely receive these different types of information directly through AstA,
593 DH44, and Lk receptor signaling, and indirectly through NPF and dopamine (DA) pathways.
594 FBl6 integrates the converging information to form a representation of choice, which is relayed
595 to downstream motor circuits for behavior implementation.

596 **Extended Table 1**

Figure	Datasets compared	Statistics
Fig. 1d	w^{1118} male vs. female Preference index	Mixed-effects analysis, $F(9,118)=22.46$, $p<0.0001$
		Sidak's adjusted p:
	1mM male vs. female (n=10) 10mM male vs. female (n=10) 50mM male vs. female (n=20) 100mM male vs. female (n=27) 500mM male vs. female (n=10)	0.9968 >0.9999 0.1784 0.5552 0.8233
Fig. 1e	w^{1118} Preference index, Group size (n=77)	Pearson's $r^2=0.05655$, $p=0.0373$
Fig. 1f	w^{1118} Preference index, % ate (n=77)	Pearson's $r^2=0.225$, $p<0.0001$
Fig. 1g	w^{1118} % ate, Group size (n=77)	Pearson's $r^2=0.0006$, $p=0.8313$
Fig. 1h	w^{1118} Preference index, Group size, % ate	Multiple linear regression, $F(3,73)=9.393$, $p<0.0001$ $r^2=0.278$

Fig. 2a	Optogenetic Screen 20XUAS-Chrimson (Chr) empty>Chr (n=30)	One-way ANOVA, F(40,358)=5.397, p<0.0001
		Dunnett's adjusted p:
	empty>Chr vs. Akh>Chr (n=10)	0.9996
	empty>Chr vs. AstA>Chr (n=10)	**<0.0001**
	empty>Chr vs. Crz>Chr (n=10)	0.9990
	empty>Chr vs. DH44>Chr (n=10)	0.1302
	empty>Chr vs. Lk>Chr (n=10)	0.9997
	empty>Chr vs. NPF>Chr (n=10)	**<0.0001**
	empty>Chr vs. Proctolin>Chr (n=10)	0.9997
	empty>Chr vs. sNPF>Chr (n=10)	0.9983
	empty>Chr vs. Tk>Chr (n=10)	0.9993
	empty>Chr vs. TH>Chr (n=10)	0.9983
	empty>Chr vs. PPL1 (504B)>Chr (n=10)	0.9998
	empty>Chr vs. PPL1 (65B)>Chr (n=10)	0.9996
	empty>Chr vs. PAM (58E02)>Chr (n=10)	0.9993
	empty>Chr vs. OA/TA Tdc>Chr (n=10)	>0.9999
	empty>Chr vs. Ser/Trh>Chr (n=10)	0.9997
	empty>Chr vs. γ2α'1>Chr (n=10)	**<0.0001**
	empty>Chr vs. α3>Chr (n=10)	0.8644
	empty>Chr vs. γ1-pedc>Chr (n=10)	0.9986
	empty>Chr vs. α'2α2>Chr (n=10)	0.9997
	empty>Chr vs. α'2α2,γ2α'1>Chr (n=10)	0.9995
	empty>Chr vs. α1>Chr (n=10)	**0.0070**
	empty>Chr vs. β1>Chr (n=10)	0.1241
	empty>Chr vs. β1β2>Chr (n=10)	0.9924
	empty>Chr vs. γ5>Chr (n=10)	0.9997
	empty>Chr vs. β'2a>Chr (n=6)	0.9983
	empty>Chr vs. γ4,γ4<γ1γ2>Chr (n=10)	0.9982
	empty>Chr vs. γ3>Chr (n=10)	0.9990
	empty>Chr vs. allKC 10B>Chr (n=10)	0.9988
	empty>Chr vs. α/β 8B>Chr (n=8)	0.9988
	empty>Chr vs. α/β c739>Chr (n=10)	0.9988
	empty>Chr vs. α'/β' 5B>Chr (n=10)	0.9997
	empty>Chr vs. γ-m 131B>Chr (n=8)	0.3762
	empty>Chr vs. FBl4,6 ss20>Chr (n=15)	0.9997
	empty>Chr vs. FBl3,4,6 ss208>Chr (n=10)	0.9990
	empty>Chr vs. FBl3,4,6 ss225>Chr (n=10)	0.9993
	empty>Chr vs. FBl6 c205>Chr (n=10)	0.9777
	empty>Chr vs. FBl2,8,9 R89E07>Chr (n=10)	0.6555
	empty>Chr vs. FBl5,8,9 R38E07>Chr (n=10)	0.9994
	empty>Chr vs. ventral FB R58F03>Chr (n=10)	0.3548
	empty>Chr vs. FBl1,2 R52G12>Chr (n=10)	0.9987

Fig. 2a	Optogenetic Screen 20XUAS-GtACR1 (Gt) empty>Gt (n=30)	One-way ANOVA, F(10,129)=7.719, p<0.0001
		Dunnett's adjusted p:
	empty>Gt vs. AstA>Gt (n=10) **empty>Gt vs. DH44>Gt** (n=10) **empty>Gt vs. Lk>Gt** (n=10) empty>Gt vs. NPF>Gt (n=10) empty>Gt vs. γ2α'1>Gt (n=10) **empty>Gt vs. α3>Gt1** (n=10) empty>Gt vs. α1>Gt (n=10) empty>Gt vs. β1>Gt (n=10) **empty>Gt vs. FBl6 c205>Gt** (n=10) empty>Gt vs. FBl2,8,9 89E07>Gt (n=20)	**0.0004** **0.0023** **0.0081** 0.4307 >0.9999 **<0.0001** 0.9628 0.9996 **0.0002** 0.2042
Fig. 2b	Lk (left panel)	One-way ANOVA, F(4,84)=8.136, p<0.0001
		Sidak's adjusted p:
	empty>Chr (n=10) (n=10) vs. Lk>Chr (n=20) empty>Chr (n=10) vs. Lk>UAS-Chr;UAS-DH44^{RNAi} (n=30) **empty>Gt** (n=10) **vs. Lk>Gt** (n=19)	0.2664 0.3550 **0.0005**
Fig. 2b	Lk (right panel) RNAi ctrl = Lk-GAL4>UAS-Valium (n=20)	One-way ANOVA, F(7,106)=1.973, p=0.0655
	RNAi ctrl vs. AstA-R1^{RNAi} (n=14) RNAi ctrl vs. DH44-R1^{RNAi} (n=10) RNAi ctrl vs. NPFR^{RNAi} (n=10) RNAi ctrl vs. Dop1R1^{RNAi} (n=20) RNAi ctrl vs. Dop1R2^{RNAi} (n=10) RNAi ctrl vs. Dop2R^{RNAi} (n=20) RNAi ctrl vs. DopEcR^{RNAi} (n=10)	Multiple comparisons not carried out since ANOVA is not significant
Fig. 2c	AstA (left panel)	One-way ANOVA, F(4,75)=61.57, p<0.0001
		Sidak's adjusted p:
	empty>Chr (n=10) **vs. Chr** (n=20) empty>Chr (n=10) vs. AstA>UAS-Chr;UAS-AstA^{RNAi} (n=20) **empty>Gt** (n=10) **vs. AstA>Gt** (n=20)	**<0.0001** 0.9814 **<0.0001**
Fig. 2c	AstA (right panel) RNAi ctrl = AstA-GAL4>UAS-Valium (n=20)	One-way ANOVA, F(7,90)=4.368, p=0.0003
		Dunnett's adjusted p:
	RNAi ctrl vs. DH44-R1^{RNAi} (n=10)	0.9530

	RNAi ctrl vs. Lkr^{RNAi} (n=5) RNAi ctrl vs. NPFR^{RNAi} (n=13) **RNAi ctrl vs. Dop1R1^{RNAi}** (n=20) RNAi ctrl vs. Dop1R2^{RNAi} (n=10) RNAi ctrl vs. Dop2R^{RNAi} (n=10) RNAi ctrl vs. DopEcR^{RNAi} (n=10)	0.2010 0.5986 **0.0005** 0.9998 0.9979 0.9975
Fig. 2d	NPF (left panel)	One-way ANOVA, F(5,89)=11.81, p<0.0001
		Sidak's adjusted p:
	empty>Chr (n=10) **vs. NPF>Chr** (n=20) empty>Chr (n=10) vs. NPF>UAS-Chr;UAS-NPF^{RNAi} (n=25) empty>Gt (n=10) vs. NPF>Gt (n=20)	**0.0002** 0.9855 0.1928
Fig. 2d	NPF (right panel) RNAi ctrl = NPF-GAL4>UAS-Valium (n=20)	One-way ANOVA, F(7,127)=3.657, p=0.0012
		Dunnett's adjusted p:
	RNAi ctrl vs. AstA-R1^{RNAi} (n=15) RNAi ctrl vs. DH44-R1^{RNAi} (n=10) **RNAi ctrl vs. Lkr ^{RNAi}** (n=20) **RNAi ctrl vs. Dop1R1^{RNAi}** (n=20) RNAi ctrl vs. Dop1R2^{RNAi} (n=20) RNAi ctrl vs. Dop2R^{RNAi} (n=20) RNAi ctrl vs. DopEcR^{RNAi} (n=10)	0.4148 0.9972 **0.0188** **0.0026** 0.1588 0.9212 0.9910
Fig. 2e	DH44 (left panel)	One-way ANOVA, F(4,75)=10.54, p<0.0001
		Sidak's adjusted p:
	empty>Chr (n=10) vs. DH44>Chr (n=20) empty>Chr (n=10) vs. DH44>UAS-Chr;UAS-DH44^{RNAi} (n=20) **empty>Gt** (n=10) **vs. DH44>Gt** (n=20)	0.1591 0.9807 **<0.0001**
Fig. 2e	DH44 (right panel) RNAi ctrl = DH44-GAL4>UAS-Valium (n=20)	One-way ANOVA, F(7,141)=5.56, p<0.0001
		Dunnett's adjusted p:
	RNAi ctrl vs. DH44>AstA-R1^{RNAi} (n=20) RNAi ctrl vs. DH44>Lkr^{RNAi} (n=20) RNAi ctrl vs. DH44>NPFR^{RNAi} (n=19) RNAi ctrl vs. DH44>Dop1R1^{RNAi} (n=20) RNAi ctrl vs. DH44>Dop1R2^{RNAi} (n=10) RNAi ctrl vs. DH44>Dop2R^{RNAi} (n=20) **RNAi ctrl vs. DH44>DopEcR^{RNAi}** (n=20)	0.7806 0.6273 0.9997 0.9998 0.9996 0.9952 **0.0001**

Fig. 3a	c205 (left panel)	One-way ANOVA, $F(14,318)=3.315$, $p<0.0001$
		Sidak's adjusted p:
	empty>Chr (n=26) vs. c205>Chr (n=45) **empty>Gt** (n=20) **vs. c205>Gt** (n=20)	0.2150 **<0.0001**
	c205 (right panel) RNAi ctrl = c205-GAL4>UAS-Valium (n=47)	Kruskal-Wallis stat=40.85, p<0.0001
		Dunn's adjusted p:
	RNAi ctrl vs. $AstA^{RNAi}$ (n=20) **RNAi ctrl vs. AstA-R1^{RNAi}** (n=20) RNAi ctrl vs. $DH44^{RNAi}$ (n=20) **RNAi ctrl vs. DH44-R1^{RNAi}** (n=20) RNAi ctrl vs. Lk^{RNAi} (n=20) **RNAi ctrl vs. Lkr^{RNAi}** (n=20) RNAi ctrl vs. NPF^{RNAi} (n=20) RNAi ctrl vs. $NPFR^{RNAi}$ (n=40) RNAi ctrl vs. $Dop1R1^{RNAi}$ (n=20) RNAi ctrl vs. $Dop1R2^{RNAi}$ (n=20) RNAi ctrl vs. $Dop2R^{RNAi}$ (n=20) RNAi ctrl vs. $DopEcR^{RNAi}$ (n=31)	0.2550 **0.0131** 0.1245 **0.0001** 0.9999 **0.0011** 0.9999 0.9999 0.9999 0.9999 0.6954 0.9999
Fig. 3b	c205 % ate	Kruskal-Wallis stat=49.98, p<0.0001
		Dunn's adjusted p:
	c205>Chr deprived (n=29) **vs. fed** (n=10) **c205>Gt deprived** (n=20) **vs. fed** (n=10)	**<0.0001** **<0.0001**
Fig. 3c	Food intake empty>Chr (n=10) c205>Chr (n=8)	Kruskal-Wallis stat=3.022, p=0.6966
Fig. 3d	Food intake empty>Gt (n=7), c205>Gt (n=7)	Kruskal-Wallis stat=4.189, p=0.5225
Fig. 3e	Place PI empty>Chr (n=8), c205>Chr (n=20) empty>Gt (n=7), c205>Gt (n=8)	One-way ANOVA, $F(3,39)=2.284$, p=0.094
Fig. 4e	Peak $\Delta R/R_0$	Kruskal-Wallis stat=56.6, p<0.0001
		Wilcoxon matched pairs p:
	naïveDeprived sweet (n=10) vs. naïveDeprived bittersweet (n=10) naïveFed sweet (n=12) vs. naïveFed bittersweet (n=12) **choseSweet sweet (n=5) vs. choseSweet bittersweet (n=5)** **choseBittersweet sweet (n=5) vs. choseBittersweet bittersweet (n=5)** choseNeither sweet (n=10) vs. choseNeither bittersweet (n=10)	**0.0244** 0.3110 **0.0310** **0.0313** 0.50

Extended Table 2

Figure	Genotype	Source
Fig. 2, 3	empty = Empty split-GAL4	FlyLight Robot ID: 3019156
Fig. 2, 3	Chr = 20XUAS-CsChrimson (X)	RRID:BDSC_55134
Fig. 2, 3	20XUAS-CsChrimson (II) for Chr;RNAi experiments	RRID:BDSC_55136
Fig. 2, 3	Gt = 20XUAS-GtACR1 (III)	Rebecca Yang (Duke), A. Claridge-Chang (Duke-NUS)
Fig. 2	Akh-GAL4	RRID:BDSC_25684
Fig. 2	AstA-GAL4	RRID:BDSC_51979
Fig. 2	Crz-GAL4	RRID:BDSC_51976
Fig. 2	DH44-GAL4	RRID:BDSC_51987
Fig. 2	Lk-GAL4	RRID:BDSC_51993
Fig. 2	NPF-GAL4	RRID:BDSC_25682
Fig. 2	Proctolin-GAL4	RRID:BDSC_51972
Fig. 2	sNPF-GAL4	RRID:BDSC_51991
Fig. 2	Tk-GAL4	RRID:BDSC_51973
Fig. 2	TH-GAL4 (ple-GAL4)	RRID:BDSC_8848
Fig. 2	(PPL1) MB504B-GAL4	RRID:BDSC_68329
Fig. 2	(PPL1) MB065B-GAL4	RRID:BDSC_68281
Fig. 2	(PAM) 58E02-GAL4	RRID:BDSC_41347
Fig. 2	Tdc-GAL4	RRID:BDSC_9313
Fig. 2	Trh-GAL4	RRID:BDSC_38388
Fig. 2	(PPL1-γ2α'1) MB296B-GAL4[8,9]	RRID:BDSC_68308
Fig. 2	(PPL1-α3) MB630B-GAL4[9]	RRID:BDSC_68334
Fig. 2	(PPL1-γ1-pedc) MB320C-GAL4[9]	RRID:BDSC_68253
Fig. 2	(PPL1-α'2α2) MB058B-GAL4[8]	RRID:BDSC_68278
Fig. 2	(PPL1-α'2α2, γ2α'1) MB099C-GAL4[9]	RRID:BDSC_68290
Fig. 2	(PAM-α1) MB043C-GAL4[8,9]	RRID:BDSC_68363
Fig. 2	(PAM-β1) MB063B-GAL4[8,9]	RRID:BDSC_68248
Fig. 2	(PAM-β1β2) MB213B-GAL4[8,9]	RRID:BDSC_68273
Fig. 2	(PAM-γ5) MB315C-GAL4[8,9]	RRID:BDSC_68316
Fig. 2	(PAM-β'2a) MB109B-GAL4[8,9]	RRID:BDSC_68261
Fig. 2	(PAM-γ4,γ4< γ1γ2) MB312C-GAL4[8]	RRID:BDSC_68252
Fig. 2	(PAM-γ3) MB441B-GAL4[8]	RRID:BDSC_68251
Fig. 2	(all KC) MB010B-GAL4[8]	FlyLight Robot ID: 2135061
Fig. 2	(α/β KC) MB008B-GAL4[8]	FlyLight Robot ID: 2135059
Fig. 2	(α/β KC) c739-GAL4	RRID:BDSC_7362
Fig. 2	(α'/β' KC) MB005B-GAL4[8]	FlyLight Robot ID: 2135056
Fig. 2	(γ-m KC) MB131B-GAL4[8]	FlyLight Robot ID: 2135179
Fig. 2	(FBl4,6) ss20-GAL4 (III)	L. Shao, U. Heberlein, FlyLight

Fig. 2	(FBl4,6) ss208-GAL4 (III)	A. Jenett, T. Wolff, G. Rubin, FlyLight
Fig. 2	(FBl4,6) ss225-GAL4 (III)	A. Jenett, T. Wolff, G. Rubin, FlyLight
Fig. 2, 3	(FBl6) c205-GAL4	RRID:BDSC_30826
Fig. 2	(FBl2,8,9) 89E07-GAL4[10]	RRID:BDSC_40553
Fig. 2	(FBl5,8,9) 38E07-GAL4[10]	RRID:BDSC_50007
Fig. 2	(ventral FB) 58F03-GAL4	RRID:BDSC_39187
Fig. 2	(FBl1,2) 52G12-GAL4	RRID:BDSC_49581
Fig. 2, 3	UAS-Valium	RRID:BDSC_35786
Fig. 2, 3	UAS-Lk-RNAi[11-14]	RRID:BDSC_25798
Fig. 2, 3	UAS-Lkr-RNAi[11,13,15]	RRID:BDSC_25936
Fig. 2, 3	UAS-AstA-RNAi[14,16]	RRID:BDSC_25866
Fig. 2, 3	UAS-AstA-R1-RNAi[17]	RRID:BDSC_27280
Fig. 2, 3	UAS-NPF-RNAi[14,18,19]	RRID:BDSC_27237
Fig. 2, 3	UAS-NPFR-RNAi[13,19-21]	RRID:BDSC_25939
Fig. 2, 3	UAS-DH44-RNAi[14,22,23]	RRID:BDSC_25804
Fig. 2, 3	UAS-DH44-R1-RNAi[22]	RRID:BDSC_28780
Fig. 2, 3	UAS-Dop1R1-RNAi[21]	RRID:BDSC_62193
Fig. 2, 3	UAS-Dop1R2-RNAi[21]	RRID:BDSC_65997
Fig. 2, 3	UAS-Dop2R-RNAi[21]	RRID:BDSC_26001
Fig. 2, 3	UAS-DopEcR-RNAi[21]	RRID:BDSC_31981
Fig. 4	(FBl6) 84C10-GAL4	RRID:BDSC_48378
Fig. 4	UAS-GCaMP6f;UAS-tdTomato	D. Clark, Yale University

Extended Table 3 (Extended figure statistics):

Figure	Datasets compared	Statistics
Ext Fig. 3b	84C10-GAL4 Preference index	One-way ANOVA, F(3,50)=7.823, p=0.0002
		Sidak's adjusted p:
	84C10>Valium (n=17) vs. 84C10>Chr (n=17)	0.1463
	84C10>Valium (n=10) vs. 84C10>Gt (n=10)	**0.0034**
Ext Fig. 3c	84C10-GAL4 % ate	One-way ANOVA, F(3,55)=186.1, p<0.0001
		Sidak's adjusted p:
	deprived 84C10>Chr (n=17) vs. fed 84C10>Chr (n=15) **deprived 84C10>Gt (n=20) vs. fed 84C10>Gt (n=7)**	**<0.0001** **<0.0001**

Extended references

1 Perkins, L. A. *et al.* The Transgenic RNAi Project at Harvard Medical School: Resources and Validation. *Genetics* **201**, 843-852, doi:10.1534/genetics.115.180208 (2015).

2 Ni, J. Q. *et al.* A Drosophila resource of transgenic RNAi lines for neurogenetics. *Genetics* **182**, 1089-1100, doi:10.1534/genetics.109.103630 (2009).

3 Wong, R., Piper, M. D., Wertheim, B. & Partridge, L. Quantification of food intake in Drosophila. *PLoS One* **4**, e6063, doi:10.1371/journal.pone.0006063 (2009).

4 Deshpande, S. A. *et al.* Quantifying Drosophila food intake: comparative analysis of current methodology. *Nat Methods* **11**, 535-540, doi:10.1038/nmeth.2899 (2014).

5 Xu, C. S. *et al.* A Connectome of the Adult Drosophila Central Brain. *bioRxiv*, 2020.2001.2021.911859, doi:10.1101/2020.01.21.911859 (2020).

6 Jody, C. *et al. NeuronBridge Codebase*. (2020).

7 Meissner, G. W. *et al.* An image resource of subdivided Drosophila GAL4-driver expression patterns for neuron-level searches. *bioRxiv*, 2020.2005.2029.080473, doi:10.1101/2020.05.29.080473 (2020).

8 Aso, Y. *et al.* The neuronal architecture of the mushroom body provides a logic for associative learning. *Elife* **3**, e04577, doi:10.7554/eLife.04577 (2014).

9 Aso, Y. & Rubin, G. M. Dopaminergic neurons write and update memories with cell-type-specific rules. *Elife* **5**, doi:10.7554/eLife.16135 (2016).

10 Hu, W. *et al.* Fan-Shaped Body Neurons in the Drosophila Brain Regulate Both Innate and Conditioned Nociceptive Avoidance. *Cell Rep* **24**, 1573-1584, doi:10.1016/j.celrep.2018.07.028 (2018).

11 Cavey, M., Collins, B., Bertet, C. & Blau, J. Circadian rhythms in neuronal activity propagate through output circuits. *Nat Neurosci* **19**, 587-595, doi:10.1038/nn.4263 (2016).

12 Murphy, K. R. *et al.* Postprandial sleep mechanics in Drosophila. *Elife* **5**, doi:10.7554/eLife.19334 (2016).

13 Senapati, B. *et al.* A neural mechanism for deprivation state-specific expression of relevant memories in Drosophila. *Nat Neurosci* **22**, 2029-2039, doi:10.1038/s41593-019-0515-z (2019).

14 Lee, J. H., Bassel-Duby, R. & Olson, E. N. Heart- and muscle-derived signaling system dependent on MED13 and Wingless controls obesity in Drosophila. *Proc Natl Acad Sci U S A* **111**, 9491-9496, doi:10.1073/pnas.1409427111 (2014).

15 Zandawala, M. *et al.* Modulation of Drosophila post-feeding physiology and behavior by the neuropeptide leucokinin. *PLoS Genet* **14**, e1007767, doi:10.1371/journal.pgen.1007767 (2018).

16 Schiemann, R. *et al.* Identification and In Vivo Characterisation of Cardioactive Peptides in Drosophila melanogaster. *Int J Mol Sci* **20**, doi:10.3390/ijms20010002 (2018).

17 Yu, Y. *et al.* Regulation of starvation-induced hyperactivity by insulin and glucagon signaling in adult Drosophila. *Elife* **5**, doi:10.7554/eLife.15693 (2016).

18 Guevara, A., Gates, H., Urbina, B. & French, R. Developmental Ethanol Exposure Causes Reduced Feeding and Reveals a Critical Role for Neuropeptide F in Survival. *Front Physiol* **9**, 237, doi:10.3389/fphys.2018.00237 (2018).

19 Ameku, T. *et al.* Midgut-derived neuropeptide F controls germline stem cell proliferation in a mating-dependent manner. *PLoS Biol* **16**, e2005004, doi:10.1371/journal.pbio.2005004 (2018).

20 Tsao, C. H., Chen, C. C., Lin, C. H., Yang, H. Y. & Lin, S. Drosophila mushroom bodies integrate hunger and satiety signals to control innate food-seeking behavior. *Elife* **7**, doi:10.7554/eLife.35264 (2018).

21 Klose, M. & Shaw, P. Sleep-drive reprograms clock neuronal identity through CREB-binding protein induced PDFR expression. *bioRxiv*, 2019.2012.2012.874628, doi:10.1101/2019.12.12.874628 (2019).

22 King, A. N. *et al.* A Peptidergic Circuit Links the Circadian Clock to Locomotor Activity. *Curr Biol* **27**, 1915-1927 e1915, doi:10.1016/j.cub.2017.05.089 (2017).

23 Cannell, E. *et al.* The corticotropin-releasing factor-like diuretic hormone 44 (DH44) and kinin neuropeptides modulate desiccation and starvation tolerance in Drosophila melanogaster. *Peptides* **80**, 96-107, doi:10.1016/j.peptides.2016.02.004 (2016).

Extended figure legends

Extended Fig. 1. Wild-type fly behavior. a, w1118 flies always prefer higher sucrose concentration when no quinine is present. **b**, Food preference is sucrose concentration ratio dependent between two food options when quinine concentration is kept constant in the bittersweet food. **c**, Most w1118 flies ate at 21 h food deprivation, with almost 100% eating at the no-preference 50 mM sucrose condition. Plots depict mean with ±95% CI; violins show data distribution.

Extended Fig. 2. a, Percent of flies that ate during the optogenetic screen for all the genotypes tested. **b**, only ~4% of the flies eat when Lk neurons were activated (Lk>Chr) and this effect is abolished (~57% ate) by knocking down Lk in the same neurons during activation (Lk>Chr;Lk-RNAi). Plots depict mean with ±95% CI; violins show data distribution.

Extended Fig. 3. 84C10-GAL4 characterization. a, 84C10-GAL4 shows high baseline GCaMP6f fluorescence. Images shown are raw florescence images from the same frame without

677 background subtraction. **b**, 84C10-GAL4 shows the same behavioral phenotype as c205-GAL4
678 when optogenetically activated (84C10>Chr) and inhibited (84C10>Gt) compared to controls.
679 Flies prefer bittersweet food compared to control flies when FBl6 neurons are inhibited. **c**, Fed
680 flies do not eat on FBl6 activation or inhibition and **d-e**, the total consumption as well as sweet
681 and bittersweet consumption is not different between flies in the same trial on activation (**d**) or
682 inhibition (**e**). **f**, Neither activation nor inhibition of FBl6 is inherently rewarding or aversive
683 since there is no significant difference in place preference without food. **f**, Mean water response
684 ($\Delta R/R_0$) of flies with different past experience. Plots depict mean with ±95% CI; violins show
685 data distribution. See Extended Table 3 for statistics. $p<0.00001$=****, $p<0.0001$=***,
686 $p<0.01$=**, $p<0.05$=*.

Figure 1

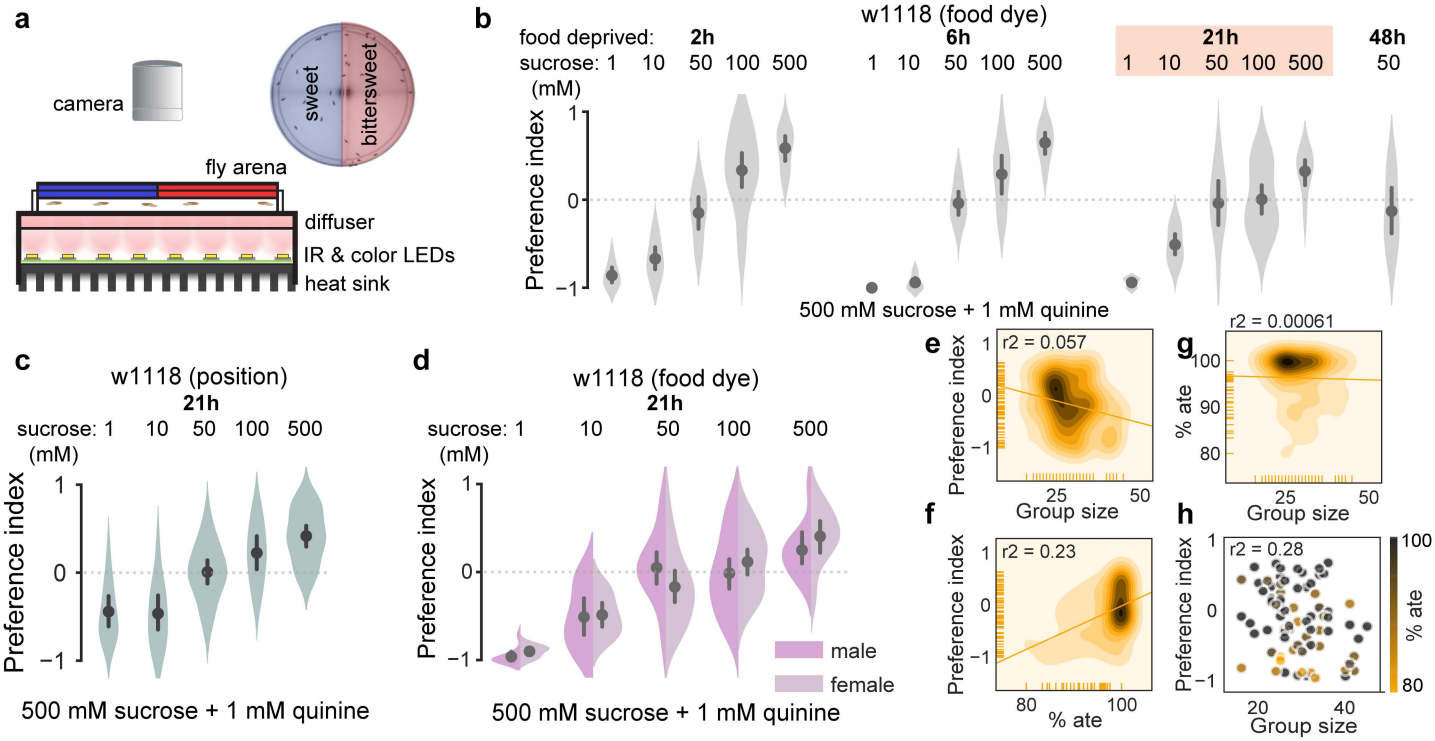

Figure 2

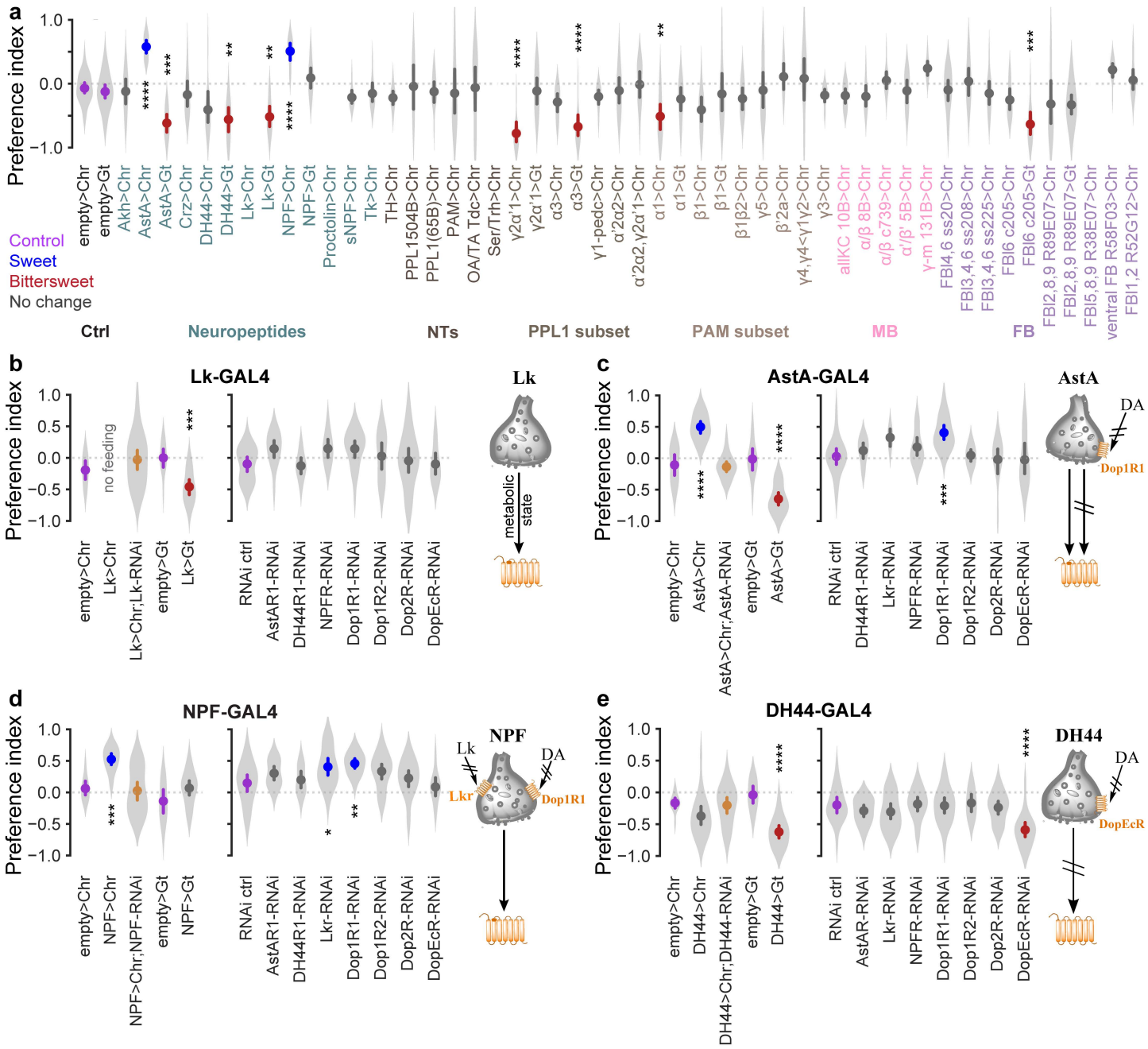

Figure 3

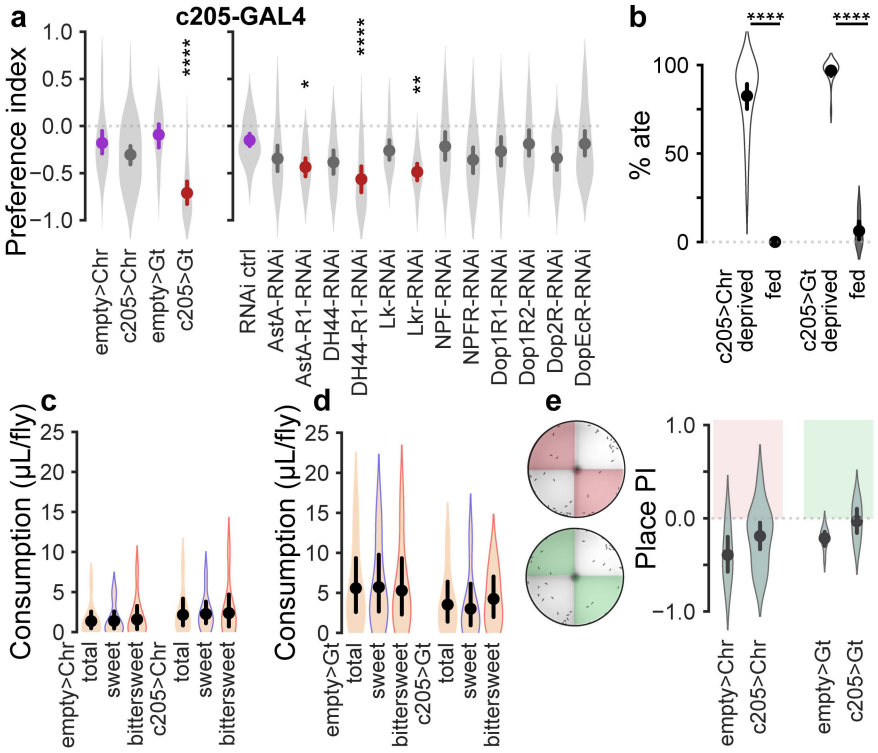

Figure 4

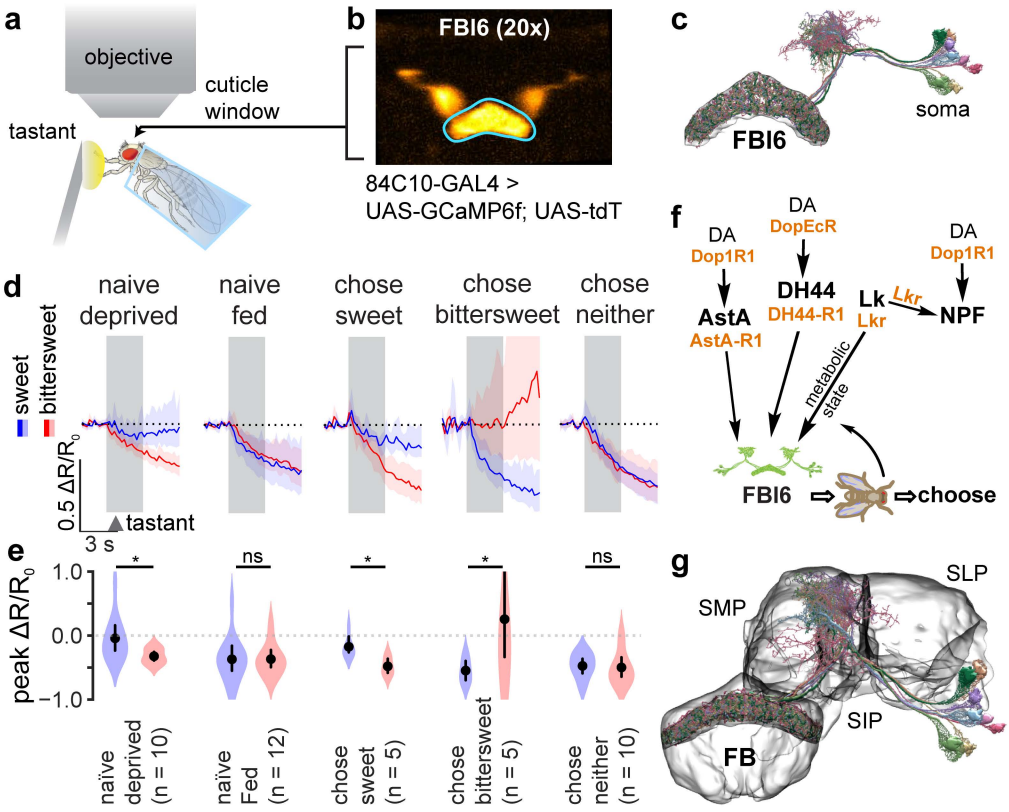

Extended figure 1

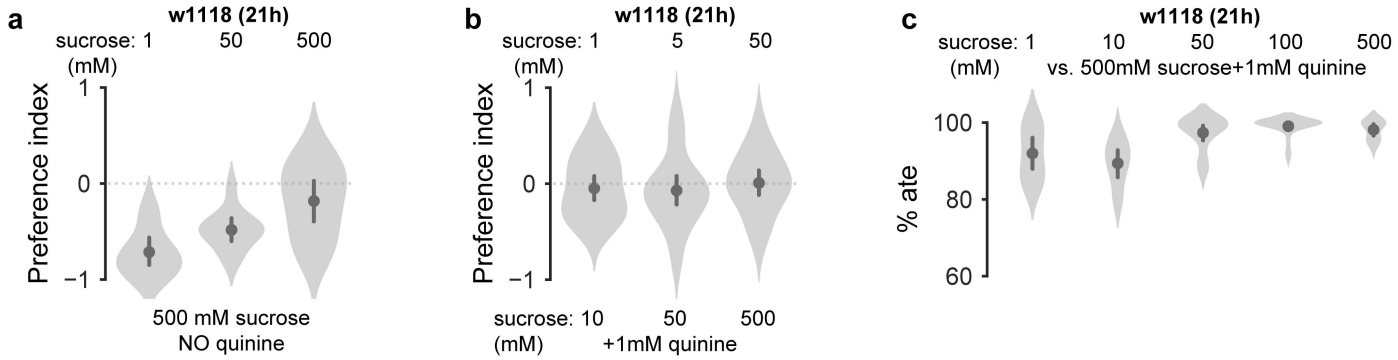

Extended figure 2

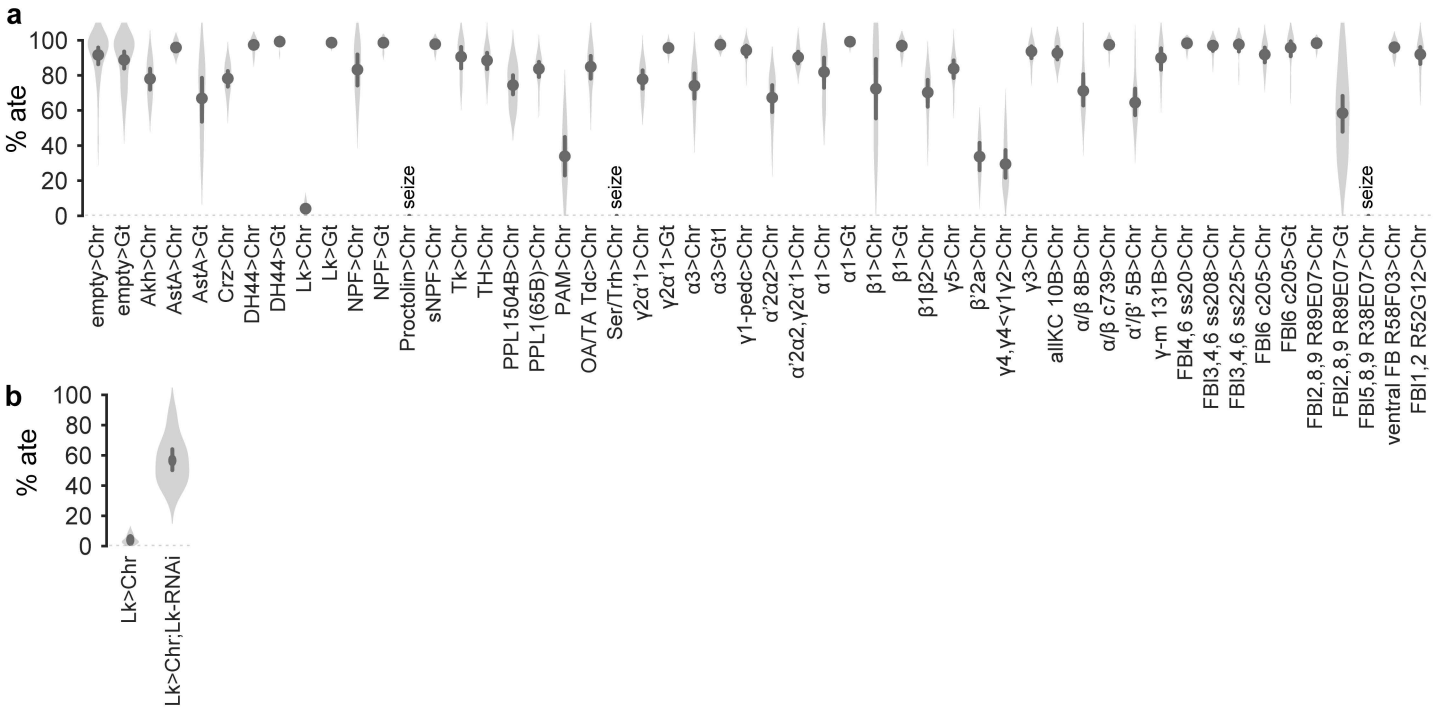

Extended figure 3